

Ultralow-temperature thermal conductivity of $\text{Pr}_2\text{Ir}_2\text{O}_7$: a metallic spin-liquid candidate with quantum criticality

J. M. Ni,¹ Y. Y. Huang,¹ E. J. Cheng,¹ Y. J. Yu,¹ B. L. Pan,¹ Q. Li,¹ L. M. Xu,² Z. M. Tian,^{2,†} and S. Y. Li^{1,3,*}

¹State Key Laboratory of Surface Physics, Department of Physics,
and Laboratory of Advanced Materials, Fudan University, Shanghai 200433, China

²School of Physics, and Wuhan National High Magnetic Field Center,
Huazhong University of Science and Technology, Wuhan 430074, China

³Collaborative Innovation Center of Advanced Microstructures, Nanjing 210093, China

(Dated: July 31, 2018)

The frustrated pyrochlore iridate $\text{Pr}_2\text{Ir}_2\text{O}_7$ was proposed as a metallic quantum spin liquid located at a zero-field quantum critical point. Here we present the ultralow-temperature thermal conductivity measurements on the $\text{Pr}_2\text{Ir}_2\text{O}_7$ single crystals to detect possible exotic excitations. In zero field, the thermal conductivity shows a dramatic suppression above a characteristic temperature $T_s \approx 0.12$ K. With increasing field, T_s increases and the thermal conductivity tends to saturate above $H = 5$ T. The Wiedemann-Franz law is verified at high fields and inferred at zero field. It suggests the normal behavior of electrons at the quantum critical point, and the absence of mobile fermionic magnetic excitations. The strong suppression of thermal conductivity is attributed to the scattering of phonons by the spin system, likely the fluctuating spins. These results shed new light on the microscopic description on this novel compound.

Spin ice state on a frustrated pyrochlore lattice has attracted numerous interests in condensed matter physics, due to the emergent magnetic monopole excitations from the manifold of degenerate ground states [1, 2]. By introducing quantum fluctuations with $J_{eff} = 1/2$ moments, quantum spin ice (QSI) states can be stabilized, exhibiting quantum electrodynamics with extra excitations like gapless photons [3–6]. $\text{Yb}_2\text{Ti}_2\text{O}_7$, $\text{Tb}_2\text{Ti}_2\text{O}_7$, and $\text{Pr}_2\text{Zr}_2\text{O}_7$ are such promising QSI candidates [3]. On the other hand, iridates with $5d$ electrons have also drawn much attention in recent years owing to the various novel quantum phases and transitions therein, which originate from the competition between spin-orbit coupling and electron-electron correlation [7, 8]. When these two aspects meet in the pyrochlore iridate $\text{Pr}_2\text{Ir}_2\text{O}_7$, complex phenomena and exotic phases emerge [9–21].

$\text{Pr}_2\text{Ir}_2\text{O}_7$ is a metal with the antiferromagnetic RKKY interaction of about 20 K in Pr $4f$ moments mediated by Ir $5d$ conduction electrons [9]. The Kondo effect leads to a partial screening of the Pr $4f$ moments and gives a lower Weiss temperature of $\theta_W = 1.7$ K [9]. No long range magnetic order was observed down to 70 mK evidenced by the magnetic susceptibility measurement, indicating a possible metallic spin liquid ground state, or even a U(1) QSI state [9, 21]. A huge and anisotropic anomalous Hall effect (AHE) was probed under magnetic fields [10, 13], which may be the results of the spin chirality effect on the Ir sites from the noncoplanar spin texture of Pr $4f$ moments. The observation of AHE in the absence of uniform magnetization at zero field further indicates a long-sought chiral spin liquid state in $\text{Pr}_2\text{Ir}_2\text{O}_7$ [11]. More interestingly, a zero-field quantum critical point (QCP) was uncovered from the diverging behavior and scaling law in the Grüneisen ratio measurement [18]. It was also theoretically investigated as a QCP between antiferroma-

gentic ordering and nodal non-Fermi liquid [19].

For such an exotic metallic spin-liquid candidate with quantum criticality, although various efforts have been made, two main issues remain to be solved in $\text{Pr}_2\text{Ir}_2\text{O}_7$. Firstly, how do the electrons behave at the QCP? In other words, will the electrons still be well-defined Landau quasiparticles? Secondly, little information is known for possible exotic magnetic excitations in $\text{Pr}_2\text{Ir}_2\text{O}_7$, probably due to the large neutron absorption cross-section of the iridium ions, and the very small size of its single crystals [22].

Ultralow-temperature thermal conductivity measurement is an important technique to address above two issues. For the former one, the verification of the Wiedemann-Franz (WF) law $\kappa/\sigma T = \pi^2 k_B^2 / 3e^2 = L_0$ can be viewed as an evidence of the survival of Landau quasiparticles at the QCP. Anomalous reduction of the Lorenz ratio $L(T)/L_0$ with $L(T) = \kappa/\sigma T$ has been observed in CeCoIn_5 [23], YbRh_2Si_2 [24], and YbAgGe [25], while in some other compounds such as CeNi_2Ge_2 [26] and $\text{Sr}_3\text{Ru}_2\text{O}_7$ [27], the WF law is verified at the QCP. For the latter one, a sizable residual linear term of thermal conductivity indicates the presence of highly mobile gapless excitations in triangular organics $\text{EtMe}_3\text{Sb}[\text{Pd}(\text{dmit})_2]_2$ [28], while no magnetic thermal conductivity was observed in another hotly debated QSL candidate YbMgGaO_4 [29].

In this Letter, we report on ultralow-temperature thermal conductivity measurements on single crystals of $\text{Pr}_2\text{Ir}_2\text{O}_7$. The WF law is verified at high fields and inferred at zero field, suggesting the normal behavior of electrons at the QCP and the absence of fermionic magnetic excitations. A huge magneto-thermal conductivity at finite temperature is found, which may result from the strong scattering of phonons by the fluctuating spins. We

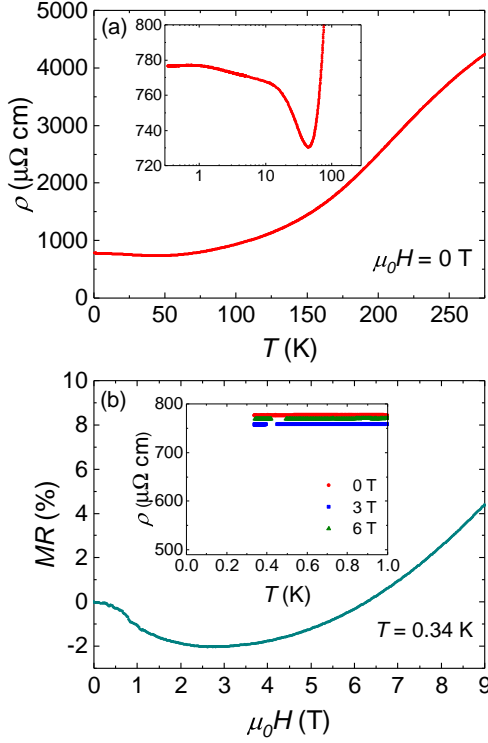


FIG. 1. (a) Temperature dependence of the resistivity at zero field of $\text{Pr}_2\text{Ir}_2\text{O}_7$ single crystal. Inset: zoomed view of the resistivity minimum at 45 K due to the Kondo effect. (b) the magnetoresistance at $T = 0.34$ K. Inset: $\rho(T)$ below 1 K in $\mu_0H = 0, 3,$ and 6 T.

shall discuss the implications of these results.

High-quality single crystals of $\text{Pr}_2\text{Ir}_2\text{O}_7$ were grown by the KF flux methods [22]. The x-ray diffraction (XRD) measurement determined the largest surface to be the (111) plane (see Supplemental Material [30]). One $\text{Pr}_2\text{Ir}_2\text{O}_7$ single crystal (sample A) for electric and thermal conductivity measurements was cut and polished into a rectangular shape of dimensions 0.69×0.38 mm² in the (111) plane, with a thickness of 0.20 mm. The thermal conductivity was measured in a dilution refrigerator, using a standard four-wire steady-state method with two RuO_2 chip thermometers, calibrated *in situ* against a reference RuO_2 thermometer. The electric current and heat current were applied in the (111) plane.

Figure 1(a) shows the temperature dependence of the resistivity $\rho(T)$ at zero field for the $\text{Pr}_2\text{Ir}_2\text{O}_7$ single crystal. The Kondo effect is evidenced by the upturn behavior below 45 K where the resistivity displays a minimum, as shown in the inset of Fig. 1(a). This is consistent with Ref. [9]. The magnetoresistance $\text{MR} = (\rho(H) - \rho(0T))/\rho(0T) \times 100\%$ at $T = 0.34$ K is presented in Fig. 1(b). It is quite small, less than 5% up to 9 T, indicating the little influence of magnetic field on the charge transport. In the inset of Fig. 1(b), $\rho(T)$ below 1 K in $\mu_0H = 0, 3,$ and 6 T are plotted. Since all

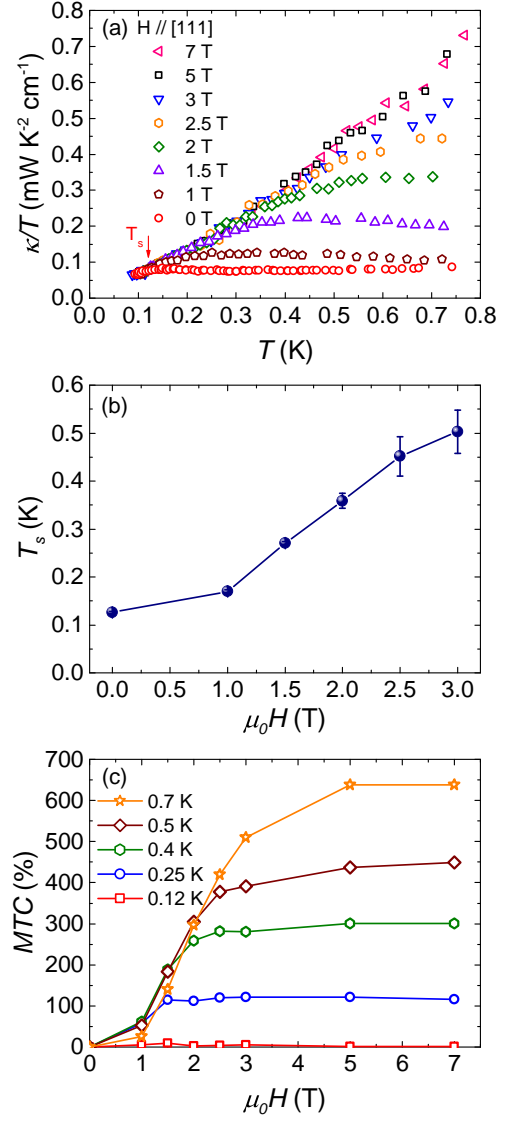


FIG. 2. (a) The thermal conductivity of $\text{Pr}_2\text{Ir}_2\text{O}_7$ single crystal at various magnetic fields along the [111] direction. At zero field, the thermal conductivity is strongly suppressed above $T_s \approx 0.12$ K. (b) Field dependence of the suppression temperature T_s . (c) The magneto-thermal conductivity $\text{MTC} = (\kappa(H) - \kappa(0T))/\kappa(0T) \times 100\%$ at various temperatures. Above 5 T, the thermal conductivity tends to saturate.

the curves are very flat, we can safely extrapolate them to the zero-temperature limit and get the residual resistivity $\rho_0 = 776, 757,$ and 769 $\mu\Omega$ cm for $\mu_0H = 0, 3,$ and 6 T, respectively.

The thermal conductivities of $\text{Pr}_2\text{Ir}_2\text{O}_7$ single crystal up to 7 T are shown in Fig. 2(a). The magnetic fields were applied perpendicular to the (111) plane. At high fields like 5 T and 7 T, the thermal conductivity data overlap with each other. With decreasing the field, while κ/T data still overlap with the high-field curves below a certain temperature T_s , they are suppressed more and

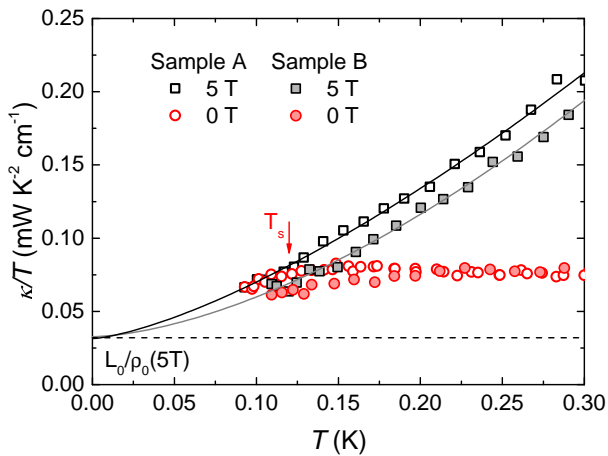


FIG. 3. The thermal conductivity of two $\text{Pr}_2\text{Ir}_2\text{O}_7$ single crystals at $\mu_0 H = 0$ and 5 T along the [111] direction, respectively. Solid lines are the fits of the thermal conductivity data to $\kappa/T = a + bT^{\alpha-1}$ at 5 T below 0.3 K. The dashed line is the Wiedemann-Franz law expectation $L_0/\rho_0(5\text{T}) = 0.032 \text{ mW K}^{-2} \text{ cm}^{-1}$ for sample A at 5 T, which meets the extrapolated $\kappa_0/T \equiv a = 0.031 \text{ mW K}^{-2} \text{ cm}^{-1}$ very well. The overlap of the 0 and 5 T curves below $T_s \approx 0.12 \text{ K}$ suggests that the Wiedemann-Franz law is also satisfied in zero field.

more strongly above T_s . At zero field, T_s is about 0.12 K. Similar behavior is also observed in another sample B (see the Supplemental Material [30]). The field-dependence of T_s is plotted in Fig. 2(b).

The magneto-thermal conductivity $\text{MTC} = \Delta\kappa(H)/\kappa(0\text{T}) = (\kappa(H) - \kappa(0\text{T}))/\kappa(0\text{T}) \times 100\%$ at various temperatures is plotted in Fig. 2(c). MTC tends to saturate above 5 T, when the thermal conductivity curves start to overlap with each other. In contrast to the magnetoresistance of less than 5% in charge transport at 0.34 K, the MTC is as large as 100% at 0.25 K and even 650% at 0.7 K. For other QSL candidates such as $\text{EtMe}_3\text{Sb}[\text{Pd}(\text{dmit})_2]_2$ [28], YbMgGaO_4 [29], and $\kappa\text{-(BEDT-TTF)}_2\text{Cu}_2(\text{CN})_3$ [31], there is also a positive MTC, but the magnitude is much smaller. We will come back to discuss the origin of this huge MTC later.

In Fig. 3, we fit the thermal conductivity data below 0.3 K for $\mu_0 H = 5 \text{ T}$ to examine the WF law in $\text{Pr}_2\text{Ir}_2\text{O}_7$. At ultra-low temperatures, thermal conductivity usually can be fitted to $\kappa/T = a + bT^{\alpha-1}$, where aT represents electrons and other fermionic quasiparticles such as spinons, while bT^α represents phonons and magnons [32, 33]. For phonons, the power α is typically between 2 and 3, due to the specular reflections at the sample surfaces [32, 33]. The fitting gives $\kappa_0/T \equiv a = 0.031 \pm 0.008 \text{ mW K}^{-2} \text{ cm}^{-1}$ and $\alpha = 2.41 \pm 0.13$ for sample A. From Fig. 1(b), $\rho_0(5\text{T}) = 764 \mu\Omega \text{ cm}$ is estimated, giving the WF law expectation $L_0/\rho_0(5\text{T}) = 0.032 \text{ mW K}^{-2} \text{ cm}^{-1}$. Therefore, the WF law is satisfied nicely. In order to confirm this result, the data of another sample B are also plotted in Fig. 3. The fitting

gives $\kappa_0/T = 0.033 \pm 0.006 \text{ mW K}^{-2} \text{ cm}^{-1}$ and $\alpha = 2.62 \pm 0.12$. Since it has $\rho_0(5\text{T}) = 755 \mu\Omega \text{ cm}$, thus $L_0/\rho_0(5\text{T}) = 0.032 \text{ mW K}^{-2} \text{ cm}^{-1}$, the WF law is also verified in sample B. The verification of WF law above $\mu_0 H = 5 \text{ T}$ is reasonable, because the magnetization approaches saturation [11] and the system is away from the QCP [18] at high field. As a result, the thermal conductivity above $\mu_0 H = 5 \text{ T}$ is purely contributed from normal electrons and phonons, without other exotic excitations or magnetic scattering.

Since the thermal conductivity data at low fields collapse on the high-field data below T_s (see Fig. 2(a)) and the MR is less than 2% for $\mu_0 H \leq 5 \text{ T}$ (see Fig. 1(b)), it would be inferred that the WF law is obeyed at all the applied fields, even at zero field. This result is significant. For $\text{Pr}_2\text{Ir}_2\text{O}_7$, a zero-field QCP was revealed by magnetic Grüneisen ratio measurements [18]. Violation of the WF law has been observed in CeCoIn_5 , YbRh_2Si_2 , and YbAgGe at their QCPs [23–25], indicating the breakdown of electrons as Landau quasiparticles. It was interpreted as a consequence of the destruction of Fermi surface [23] or the inelastic scattering [24, 25] associated with quantum critical fluctuations. The verification of the WF law in $\text{Pr}_2\text{Ir}_2\text{O}_7$ at its QCP unambiguously excludes the possibility of the breakdown of Landau quasiparticles and implies the normal formalism of electrons. This is similar to the situation in some other quantum-critical compounds such as CeNi_2Ge_2 [26] and $\text{Sr}_3\text{Ru}_2\text{O}_7$ [27].

The verification of WF law in $\text{Pr}_2\text{Ir}_2\text{O}_7$ demonstrates that there is no additional contribution to the thermal conductivity from mobile fermionic magnetic excitations. Furthermore, since the phonon thermal conductivity in high fields defines the upper boundary of κ in $\text{Pr}_2\text{Ir}_2\text{O}_7$, there is also no positive contribution to κ from other bosonic magnetic excitations. For pyrochlore $\text{Pr}_2\text{Ir}_2\text{O}_7$, one scenario to describe its possible QSL state is the QSI [3, 21]. Three topological excitations, including photon, vison, and magnetic monopole, may emerge from the ground state [3–5]. The gapless photons have a rather narrow bandwidth, about 1/1000 of the spin exchange constant J_{zz} [6]. Since J of $\text{Pr}_2\text{Ir}_2\text{O}_7$ is only 1.4 K [11], the photons are likely beyond the accessible temperature regime of our experiment. Both visons and magnetic monopoles have a gap [3–5]. It has been claimed that the thermally excited magnetic monopoles contribute to the thermal conductivity in the QSI candidates $\text{Yb}_2\text{Ti}_2\text{O}_7$ [36] and $\text{Pr}_2\text{Zr}_2\text{O}_7$ [37]. However, here in $\text{Pr}_2\text{Ir}_2\text{O}_7$, we do not observe their positive contribution. If the magnetic monopoles indeed exist in $\text{Pr}_2\text{Ir}_2\text{O}_7$ with a gap comparable to J , the thermally excited magnetic monopoles should be detectable in our temperature range. One possibility is that the velocity and/or mean free path of these excitations may be too small so that their contribution to κ is negligible comparing to that of phonons. Another possibility is that the QSI can not describe the ground

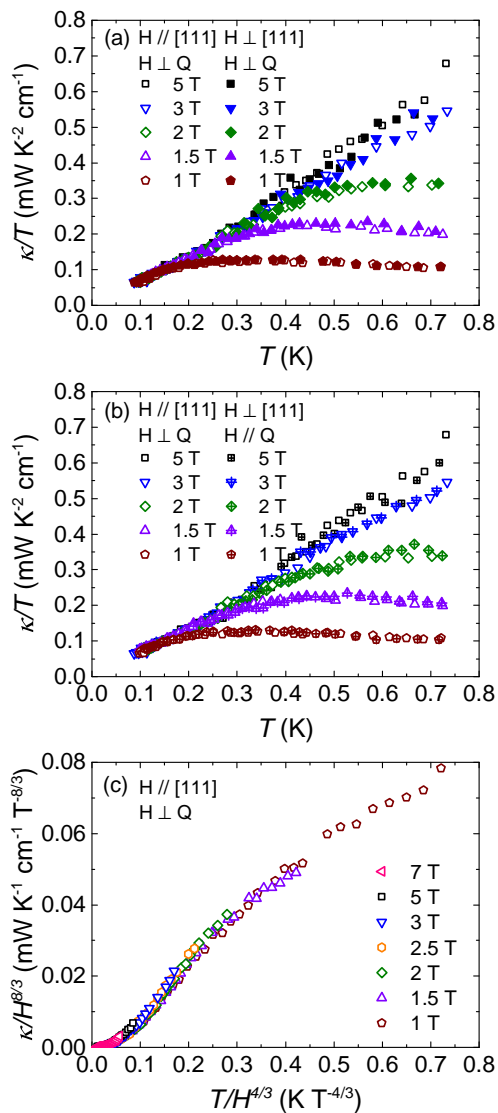


FIG. 4. (a) The thermal conductivities of $\text{Pr}_2\text{Ir}_2\text{O}_7$ single crystal in magnetic fields $H \parallel [111]$ and $H \perp Q$ are compared with those in $H \perp [111]$ and $H \perp Q$. (b) They are also compared with those in $H \perp [111]$ and $H \parallel Q$. See Supplemental Material [30] for schematic illustrations of these three geometries. The overlap of these curves in all three field directions show that the MTC is isotropic. (c) Scaling plot of the thermal conductivity. The plots of $\kappa/H^{8/3}$ versus $T/H^{4/3}$ at various magnetic fields parallel to the [111] direction collapse on the same curve.

state of $\text{Pr}_2\text{Ir}_2\text{O}_7$ thus above-mentioned magnetic excitations do not exist.

Now let us discuss the origin of the huge MTC in $\text{Pr}_2\text{Ir}_2\text{O}_7$. In Fig. 2(a), starting from the phonon thermal conductivity in high fields, the strong suppression of κ at low fields apparently comes from the scattering of phonons by the spin system through the spin-lattice coupling [34, 35], either by well-defined magnetic excitations or by fluctuating spins. In case that there are thermally

excited magnetic quasiparticles to scatter the phonons above T_s , the field dependence of T_s in Fig. 2(b) suggests that the gap (larger than T_s) of these magnetic quasiparticles increases with increasing the field. For above-mentioned magnetic monopoles, the scattering between phonons and monopoles accompanies a spin-flip process, which should be sensitive to the direction of field. Indeed, a metamagnetic transition can be induced only when applying the field along the [111] direction [11]. In order to examine this possibility, we measure the thermal conductivity in other two different field directions and compare to the [111] direction, as shown in Figs. 4(a) and 4(b). One can see that the curves in all three field directions overlap with each other. It shows that the MTC is isotropic, i.e., insensitive to the direction of field. Furthermore, the gap of magnetic monopoles should decrease with increasing the field [2], which contrasts to the field dependence of T_s . Therefore, the scattering of phonons is unlikely from magnetic monopoles. It will be interesting to theoretically investigate whether there are some other magnetic excitations beyond the QSI scenario. Their gap should be isotropic, and increase with increasing the field.

In case that there are no well-defined magnetic excitations in $\text{Pr}_2\text{Ir}_2\text{O}_7$, the strong scattering of phonons at low fields may be associated with the fluctuating spins. Intuitively, the spin fluctuations are weakened with lowering the temperature and increasing the field. For $\text{Pr}_2\text{Ir}_2\text{O}_7$, a bifurcation of the field-cooled and zero-field-cooled magnetic susceptibility curves at about 0.3 K suggests that a partial fraction of spins freezes [9, 11]. Spin freezing has also been observed in classical spin ice like $\text{Dy}_2\text{Ti}_2\text{O}_7$, and the freezing temperature increases with applying field [38, 39]. Therefore, this scenario may explain the temperature and field dependence of thermal conductivity in $\text{Pr}_2\text{Ir}_2\text{O}_7$. In each field, the spins fluctuate very slowly below T_s , partially frozen, so that they do not scatter phonons. The field will further weaken the spin fluctuations, thus the T_s increases with increasing field. The spin fluctuations is also isotropic in response to the applied field. Such a simple scenario was used to interpret the thermal conductivity of YbMgGaO_4 [29]. One may consider whether it can also apply to the heat transport behavior of other QSI candidates such as $\text{Pr}_2\text{Zr}_2\text{O}_7$ [37], as recently pointed out by Rau and Gingras in Ref. [40].

Interestingly, an unusual scaling behavior $\kappa \sim H^{8/3} F(T/H^{4/3})$, where $F(x)$ is the scaling function, is observed, as shown in Fig. 4(c). It is also held for sample B (see Supplemental Material [30]). Note that the scaling law was previously found in the magnetic Grüneisen ratio $\Gamma_H H$ versus $T/H^{4/3}$ under 2 T, implying a critical physics in $\text{Pr}_2\text{Ir}_2\text{O}_7$ [18]. Observation of the scaling law in the thermal conductivity is appealing since it is rather rare that the heat transport data scale as a function of a single parameter. Due to the unique metallic nature of $\text{Pr}_2\text{Ir}_2\text{O}_7$, which is distinct from any other in-

ulating QSL candidates, the interactions between Pr $4f$ moments and Ir $5d$ itinerant electrons may complicate the microscopic description. The scaling law gives a new viewpoint towards such quantum magnets that we hope will stimulate the theoretical study. Other experimental techniques, such as thermal Hall measurement and inelastic neutron scattering, are highly desired to determine the ground state and emergent excitations in this exotic metallic QSL candidate $\text{Pr}_2\text{Ir}_2\text{O}_7$.

In summary, we have measured the ultralow-temperature thermal conductivity of $\text{Pr}_2\text{Ir}_2\text{O}_7$ single crystals. The Wiedemann-Franz law is verified at high magnetic fields and inferred at zero field, suggesting the normal behavior of electrons at the zero-field quantum critical point and the absence of mobile fermionic magnetic excitations. A huge isotropic magneto-thermal conductivity is found at finite temperatures, indicating the strong scattering of phonons by the spin system, likely the fluctuating spins. The observed scaling law may help put constraints on the theoretical modelling on $\text{Pr}_2\text{Ir}_2\text{O}_7$. These results will shed light on the microscopic description on this metallic quantum spin liquid candidate.

We thank Z. Y. Meng, Y. Wan, Y. Zhou for helpful discussions. This work is supported by the Ministry of Science and Technology of China (Grant No: 2015CB921401 and 2016YFA0300503), the Natural Science Foundation of China, the NSAF (Grant No: U1630248), and the fundamental research funds for central universities (2018KFYYXJJ038).

† E-mail: tianzhaoming@hust.edu.cn

* E-mail: shiyang_li@fudan.edu.cn

-
- [1] L. Balents, Spin liquids in frustrated magnets, *Nature (London)* **464**, 199 (2010).
- [2] C. Castelnovo, R. Moessner, and S. L. Sondhi, Magnetic monopoles in spin ice, *Nature (London)* **451**, 42 (2008).
- [3] M. J. P. Gingras, and P. A. McClarty, Quantum spin ice: a search for gapless quantum spin liquids in pyrochlore magnets, *Rep. Prog. Phys.* **77**, 056501 (2014).
- [4] M. Hermele, M. P. A. Fisher, and L. Balents, Pyrochlore photons: The U(1) spin liquid in a S=1/2 three-dimensional frustrated magnet, *Phys. Rev. B* **69**, 064404 (2004).
- [5] K. A. Ross, L. Savary, B. D. Gaulin, and L. Balents, Quantum Excitations in Quantum Spin Ice, *Phys. Rev. X* **1**, 021002 (2011).
- [6] C.-J. Huang, Y. Deng, Y. Wan, and Z. Y. Meng. Dynamics of topological excitations in a model quantum spin ice, *Phys. Rev. Lett.* **120**, 167202 (2018).
- [7] W. Witczak-Krempa, G. Chen, Y. B. Kim, and L. Balents. Correlated Quantum Phenomena in the Strong Spin-Orbit Regime, *Annu. Rev. Condens. Matter Phys.* **5**, 57 (2014).
- [8] G. Cao and P. Schlottmann. The challenge of spin-orbit-tuned ground states in iridates: a key issues review, *Rep. Prog. Phys.* **81**, 042502 (2018).
- [9] S. Nakatsuji, Y. Machida, Y. Maeno, T. Tayama, T. Sakakibara, J. van Duijn, L. Balicas, J. N. Millican, R. T. Macaluso, and J. Y. Chan. Metallic Spin-Liquid Behavior of the Geometrically Frustrated Kondo Lattice $\text{Pr}_2\text{Ir}_2\text{O}_7$, *Phys. Rev. Lett.* **96**, 087204 (2006).
- [10] Y. Machida, S. Nakatsuji, Y. Maeno, T. Tayama, T. Sakakibara, and S. Onoda. Unconventional Anomalous Hall Effect Enhanced by a Noncoplanar Spin Texture in the Frustrated Kondo Lattice $\text{Pr}_2\text{Ir}_2\text{O}_7$, *Phys. Rev. Lett.* **98**, 057203 (2007).
- [11] Y. Machida, S. Nakatsuji, S. Onoda, T. Tayama, and T. Sakakibara. Time-reversal symmetry breaking and spontaneous Hall effect without magnetic dipole order, *Nature (London)* **463**, 210 (2010).
- [12] S. Onoda and Y. Tanaka. Quantum Melting of Spin Ice: Emergent Cooperative Quadrupole and Chirality, *Phys. Rev. Lett.* **105**, 047201 (2010).
- [13] L. Balicas, S. Nakatsuji, Y. Machida, and S. Onoda. Anisotropic Hysteretic Hall Effect and Magnetic Control of Chiral Domains in the Chiral Spin States of $\text{Pr}_2\text{Ir}_2\text{O}_7$, *Phys. Rev. Lett.* **106**, 217204 (2011).
- [14] M. Udagawa and R. Moessner. Anomalous Hall Effect from Frustration-Tuned Scalar Chirality Distribution in $\text{Pr}_2\text{Ir}_2\text{O}_7$, *Phys. Rev. Lett.* **111**, 036602 (2013).
- [15] R. Flint and T. Senthil. Chiral RKKY interaction in $\text{Pr}_2\text{Ir}_2\text{O}_7$, *Phys. Rev. B* **87**, 125147 (2013).
- [16] G. Chern, S. Maiti, R. M. Fernandes, and P. Wolfle. Electronic Transport in the Coulomb Phase of the Pyrochlore Spin Ice, *Phys. Rev. Lett.* **110**, 146602 (2013).
- [17] S. Lee, A. Paramakanti, and Y. B. Kim. RKKY Interactions and the Anomalous Hall Effect in Metallic Rare-Earth Pyrochlores, *Phys. Rev. Lett.* **111**, 196601 (2013).
- [18] Y. Tokiwa, J. J. Ishikawa, S. Nakatsuji, and P. Gegenwart. Quantum criticality in a metallic spin liquid, *Nat. Mater.* **13**, 356 (2014).
- [19] L. Savary, E. -G. Moon, and L. Balents. New Type of Quantum Criticality in the Pyrochlore Iridates, *Phys. Rev. X* **4**, 041027 (2014).
- [20] T. Kondo, M. Nakayama, R. Chen, J.J. Ishikawa, E.-G. Moon, T. Yamamoto, Y. Ota, W. Malaeb, H. Kanai, Y. Nakashima, Y. Ishida, R. Yoshida, H. Yamamoto, M. Matsunami, S. Kimura, N. Inami, K. Ono, H. Kumigashira, S. Nakatsuji, L. Balents, and S. Shin. Quadratic Fermi node in a 3D strongly correlated semimetal. *Nat. Commun.* **6**, 10042 (2015).
- [21] G. Chen. Magnetic monopole condensation of the pyrochlore ice U(1) quantum spin liquid: Application to $\text{Pr}_2\text{Ir}_2\text{O}_7$ and $\text{Yb}_2\text{Ti}_2\text{O}_7$. *Phys. Rev. B* **94**, 205107 (2016).
- [22] J. N. Millican, R. T. Macaluso, S. Nakatsuji, Y. Machida, Y. Maeno, and J. Y. Chan. Crystal growth and structure of $\text{R}_2\text{Ir}_2\text{O}_7$ (R = Pr, Eu) using molten KF. *Mater. Res. Bull.* **42**, 928 (2007).
- [23] M. A. Tanatar, J. Paglione, C. Petrovic, and L. Taillefer. Anisotropic Violation of the Wiedemann-Franz Law at a Quantum Critical Point, *Science* **316**, 1320 (2007).
- [24] H. Pfau, S. Hartmann, U. Stockert, P. Sun, S. Lausberg, M. Brando, S. Friedemann, C. Krellner, C. Geibel, S. Wirth, S. Kirchner, E. Abrahams, Qimiao Si, and F. Steglich. Thermal and electrical transport across a magnetic quantum critical point, *Nature (London)* **484**, 493 (2012).
- [25] J. K. Dong, Y. Tokiwa, S. L. Bud'ko, P. C. Canfield, and

- P. Gegenwart. Anomalous Reduction of the Lorenz Ratio at the Quantum Critical Point in YbAgGe, *Phys. Rev. Lett.* **110**, 176402 (2013).
- [26] S. Kambe, H. Suderow, T. Fukuhara, J. Flouquet, and T. Takimoto. Spin-Fluctuation Mediated Thermal Conductivity Around the Magnetic Instability of CeNi₂Ge₂, *J. Low. Temp. Phys.* **117** 101 (1999).
- [27] F. Ronning, R. W. Hill, M. Sutherland, D. G. Hawthorn, M. A. Tanatar, J. Paglione, Louis Taillefer, M. J. Graf, R. S. Perry, Y. Maeno, and A. P. Mackenzie. Thermal Conductivity in the Vicinity of the Quantum Critical End Point in Sr₃Ru₂O₇, *Phys. Rev. Lett.* **97**, 067005 (2006).
- [28] M. Yamashita, N. Nakata, Y. Senshu, M. Nagata, H. M. Yamamoto, R. Kato, T. Shibauchi, and Y. Matsuda, Highly Mobile Gapless Excitations in a Two-Dimensional Candidate Quantum Spin Liquid, *Science* **328**, 246 (2010).
- [29] Y. Xu, J. Zhang, Y. S. Li, Y. J. Yu, X. C. Hong, Q. M. Zhang, and S. Y. Li, Absence of Magnetic Thermal Conductivity in the Quantum Spin-Liquid Candidate YbMgGaO₄, *Phys. Rev. Lett.* **117**, 267202 (2016).
- [30] See Supplemental Material for XRD pattern, details about Sample B and additional analysis.
- [31] M. Yamashita, N. Nakata, Y. Kasahara, T. Sasaki, N. Yoneyama, N. Kobayashi, S. Fujimoto, T. Shibauchi, and Y. Matsuda, Thermal-transport measurements in a quantum spin-liquid state of the frustrated triangular magnet κ -(BEDT-TTF)₂Cu₂(CN)₃, *Nat. Phys.* **5**, 44 (2009).
- [32] M. Sutherland, D. G. Hawthorn, R. W. Hill, F. Ronning, S. Wakimoto, H. Zhang, C. Proust, E. Boaknin, C. Lupien, L. Taillefer, R. X. Liang, D. A. Bonn, W. N. Hardy, R. Gagnon, N. E. Hussey, T. Kimura, M. Nohara, and H. Takagi, Thermal conductivity across the phase diagram of cuprates: Low-energy quasiparticles and doping dependence of superconducting gap, *Phys. Rev. B* **67**, 174520 (2003).
- [33] S. Y. Li, J. B. Bonnemaïson, A. Payeur, P. Fournier, C. H. Wang, X. H. Chen, and L. Taillefer, Low-temperature phonon thermal conductivity of single crystalline Nd₂CuO₄: Effects of sample size and surface roughness, *Phys. Rev. B* **77**, 134501 (2008).
- [34] O. Tchernyshyov and G. W. Chern, *Introduction to Frustrated Magnetism*. (Springer, Berlin, Heidelberg, 2013)
- [35] S. Lee and E. -G. Moon. Spin-Lattice Coupling in U(1) Quantum Spin Liquids, arXiv1802.05280.
- [36] Y. Tokiwa, T. Yamashita¹, M. Udagawa, S. Kittaka, T. Sakakibara, D. Terazawa¹, Y. Shimoyama¹, T. Terashima, Y. Yasui, T. Shibauchi, and Y. Matsuda. Possible observation of highly itinerant quantum magnetic monopoles in the frustrated pyrochlore Yb₂Ti₂O₇, *Nat. Commun.* **7**, 10807 (2016).
- [37] Y. Tokiwa, T. Yamashita, D. Terazawa, K. Kimura, Y. Kasahara, T. Onishi, Y. Kato, M. Halim, P. Gegenwart, T. Shibauchi, S. Nakatsuji, E.-G Moon, and Y. Matsuda. Discovery of Emergent Photon and Monopoles in a Quantum Spin Liquid. *J. Phys. Soc. Jpn.* **87**, 064702 (2018).
- [38] J. Snyder, J. S. Slusky, R. J. Cava, and P. Schiffer. How spin ice freezes, *Nature (London)* **413**, 48 (2001).
- [39] J. Snyder, B. G. Ueland, J. S. Slusky, H. Karunadasa, R. J. Cava, and P. Schiffer. Low-temperature spin freezing in the Dy₂Ti₂O₇ spin ice, *Phys. Rev. B* **69**, 064414 (2004).
- [40] J. G. Rau and M. J. P. Gingras, Frustrated quantum rare-earth pyrochlores, arXiv:1806.09638.

Supplemental Material for “Ultralow-temperature thermal conductivity of $\text{Pr}_2\text{Ir}_2\text{O}_7$: a metallic spin-liquid candidate with quantum criticality”

I. X-RAY DIFFRACTION MEASUREMENT

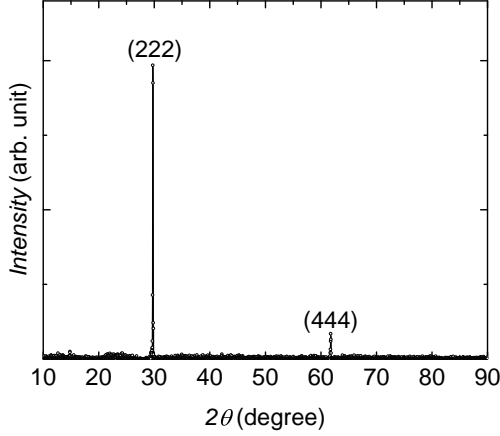


FIG. S1. Typical x-ray diffraction pattern of the $\text{Pr}_2\text{Ir}_2\text{O}_7$ single crystal.

The typical x-ray diffraction (XRD) data is plotted in Fig. S1, determining the largest surface to be the (111) plane. The heat current is applied in the (111) plane.

II. REPRODUCIBILITY OF THE TRANSPORT RESULTS

We performed transport measurements on another $\text{Pr}_2\text{Ir}_2\text{O}_7$ single crystal (Sample B), and obtained similar results to Sample A. Sample B was cut and polished into a rectangular shape with length $l = 0.72$ mm, width $w = 0.26$ mm and thickness $t = 0.20$ mm. The electric and thermal conductivity were measured by standard four-wire method.

Figure S2(a) shows the temperature dependence of the longitudinal resistivity of Sample B at zero field. The Kondo effect is also observed due to the minimum at 45 K (see bottom right inset of Fig. S2(a)), confirming the good quality of our sample. The plots of $\rho(T)$ at 0, 3, and 5 T are presented in the top left inset of Fig. S2(a). By extrapolating to the zero temperature limit, we can get the residual resistivity $\rho_0 = 757$, 749, and 755 $\mu\Omega$ cm for $\mu_0 H = 0$, 3, and 5 T, respectively.

Figure S2(b) shows the thermal conductivities of Sample B up to 7 T. The magnetic fields were applied along the [111] direction. Just as Sample A, the thermal conductivities overlap with each other and deviate from the high-field data above particular temperatures T_s . The

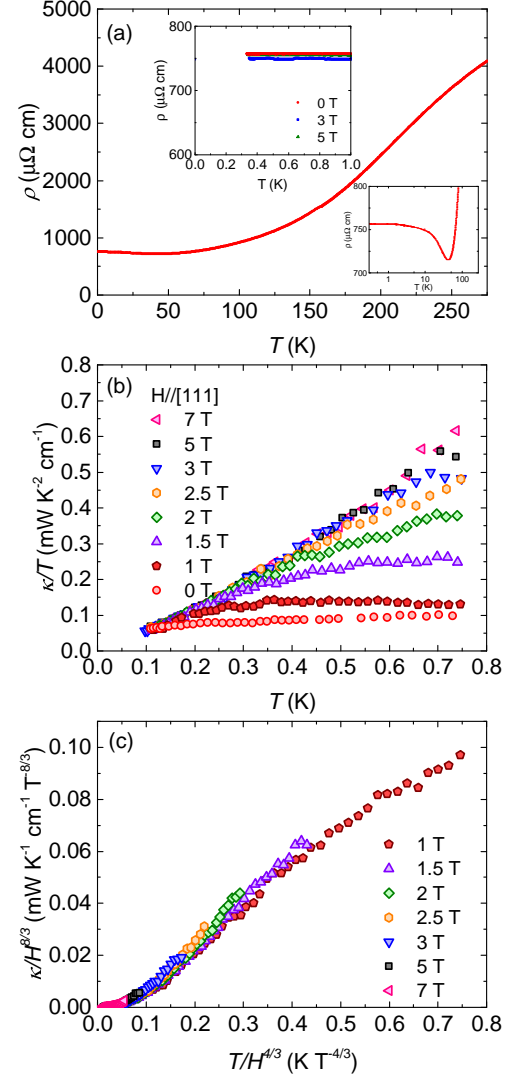


FIG. S2. (a) Temperature dependence of the resistivity of $\text{Pr}_2\text{Ir}_2\text{O}_7$ Sample B. Top left inset: $\rho(T)$ below 1 K in $\mu_0 H = 0, 3,$ and 5 T. Bottom right inset: zoomed view of the resistivity minimum at 45 K due to the Kondo effect. The magnetic fields were applied along the [111] direction. (b) The thermal conductivity of Sample B at various magnetic fields along the [111] direction. (c) Scaling plot of the thermal conductivity from Sample B. The plots of $\kappa/H^{8/3}$ versus $T/H^{4/3}$ at various magnetic fields parallel to the [111] direction collapse on the same curve.

same scaling law $\kappa \sim H^{8/3} F(T/H^{4/3})$ is also found in Sample B, see Fig. S2(c).

III. GEOMETRIES OF DIFFERENT MAGNETIC FIELD DIRECTIONS

In the main part of the paper, the thermal conductivities of $\text{Pr}_2\text{Ir}_2\text{O}_7$ single crystal in magnetic fields $H \parallel [111]$ and $H \perp Q$ are compared with those in $H \perp$

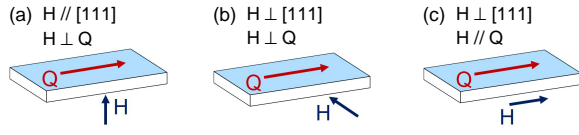


FIG. S3. (a), (b) and (c) The schematic illustrations of three different relative directions between magnetic field H (blue arrows), heat current Q (red arrows) and $[111]$ direction. The heat currents are all applied in the (111) plane, the largest surface of the sample. The (111) plane is perpendicular to the $[111]$ direction.

$[111]$ and $H \perp Q$ (Fig. 4(a) in the main part). They are also compared with the thermal conductivities in $H \perp [111]$ and $H \parallel Q$ (Fig. 4(b) in the main part). These three geometries are illustrated in Fig. S3(a), (b) and (c), respectively.